AIAA JOURNAL
Vol. 32, No. 2, February 1994

Surface Boundary Conditions for the Numerical Solution of the Euler Equations

A. Dadone*
Politecnico di Bari, 70125 Bari, Italy
and
B. Grossman†
Virginia Polytechnic Institute and State University, Blacksburg, Virginia 24061

We consider the implementation of boundary conditions at solid walls in inviscid Euler solutions by upwind, finite-volume methods. We review some current methods for the implementation of surface boundary conditions and examine their behavior for the problem of an oblique shock reflecting off a planar surface. We show the importance of characteristic boundary conditions for this problem and introduce a method of applying the classical flux-difference splitting of Roe as a characteristic boundary condition. Consideration of the equivalent problem of the intersection of two (equal and opposite) oblique shocks was very illuminating on the role of surface boundary conditions for an inviscid flow and led to the introduction of two new boundary-condition procedures, denoted as the symmetry technique and the curvature-corrected symmetry technique. Examples of the effects of the various surface boundary conditions considered are presented for the subcritical compressible flow over a circular cylinder. Dramatic advantages of the curvature-corrected symmetry technique over the other methods are shown, with regard to numerical entropy generation, total pressure loss, drag, and grid convergence.

Introduction

THE importance of surface boundary conditions in computational fluid dynamics is axiomatic. The pioneering work of Moretti[1] focused on this issue and described the inadequacies of reflection techniques, e.g., Burstein,[2] which were often utilized for finite-difference solutions in the early 1960s. A form of characteristic boundary condition was introduced by Moretti and Abbett[3] based on a discretization of the characteristic compatibility relation in time and the direction normal to the wall. This procedure significantly improved the accuracy of these early computations and many modifications and applications were made to this approach, c.f., Kentzer[4] and De Neef.[5] Moretti continued this direction with the development of the λ scheme.[6] In this scheme the surface boundary conditions are implemented by setting the time derivative of the normal velocity to zero and solving the resulting equation in terms of the spatial derivative of the characteristic variable propagating towards the wall from outside the flowfield. The characteristic boundary condition has been applied to conservative as well as nonconservative finite-difference schemes, e.g., Chakravarthy[7] and Marcum and Hoffman.[8]

For finite-volume procedures the situation is somewhat simpler in that only the pressure is required at a solid boundary. Rizzi[9] introduced a method based on a discretization of the steady-state normal momentum equation. However, modern computational fluid dynamics (CFD) methods often utilize simpler pressure-extrapolation methods, e.g., Walters and Thomas.[10] A discussion of some extrapolation methods in conjunction with finite-volume Euler calculations on Cartesian grids appears in Clark et al.[11] An attempt to include a more physical implementation of surface boundary conditions in conjunction with upwind methodologies has been performed by Deconinck and Struys.[12] They attempted to develop a Riemann solver for a solid boundary which was consistent with the interior point calculation. Their procedure worked well in conjunction with Van Leer's flux-vector splitting. The present authors[13] have examined the use of characteristic boundary conditions using Roe's flux-difference splitting for shock reflection problems.

In this paper we are concerned with the implementation of boundary conditions at solid walls in the numerical simulation of compressible inviscid flows governed by the Euler equations. We are generally concerned with steady-state solutions computed using finite-volume flow solvers involving upwind methodologies. At solid boundaries, in the absence of suction or transpiration, the normal velocity component must be set to zero. Such a condition can be fulfilled in several different ways which will be reviewed in the next section including extrapolation techniques and characteristic boundary conditions.

We will critically examine these techniques for the problem of an oblique shock reflecting off a planar surface. Consideration of the equivalent problem of the intersection of two (equal and opposite) oblique shocks was very illuminating on the role of surface boundary conditions for an inviscid flow. The importance of the characteristic boundary condition was reiterated and it will be shown that the flux-difference splitting of Roe may be implemented as a characteristic boundary condition. The equivalent problem also serves to clarify the differences between the pressure which a finite-volume flow solver uses to evaluate the surface flux and surface pressure.

Next we discuss how the previously described analysis lead us to consider the implementation of a surface boundary condition procedure, which we call a symmetry technique, and which was introduced in Ref. 14. This procedure, which is reminiscent of reflection boundary conditions for finite-difference methods, is shown to be a physically consistent technique to enforce the impermeability condition for supersonic flows with oblique shocks reflecting from plane walls.

Finally a more general boundary-condition procedure, which we call the curvature-corrected symmetry technique, is described. This method was originally introduced in Ref. 15 and is applicable to arbitrary curved geometries. We consider the subcritical compressible flow over a circular cylinder as a model problem. We show dramatic advantages of the new

Received Jan. 24, 1993; revision received July 27, 1993; accepted for publication Aug. 2, 1993.

*Professor, Istituto di Macchine ed Energetica. Senior Member AIAA.

†Professor and Head, Department of Aerospace and Ocean Engineering. Associate Fellow AIAA.

procedure with regard to numerical entropy generation and related issues of total pressure loss and drag.

Classical Impermeability Conditions

Consider the Euler equations in a Cartesian coordinate system within a semidiscrete, cell-centered, finite-volume representation of such equations, c.f., Ref. 10, and let us focus our attention on a two-dimensional, quadrilateral cell of the computational volume. The flux vector G across one of the cell faces is proportional to:

$$G \approx [\rho\tilde{v},\ \eta_x p + \rho u\tilde{v},\ \eta_y p + \rho v\tilde{v},\ \rho H\tilde{v}]^T \tag{1}$$

where u, v are the components of the velocity vector in the Cartesian coordinate system x, y; and p, ρ, and H represent the pressure, density, and total enthalpy per unit mass, respectively. Finally, $\tilde{v}$ is the velocity component normal to the cell face:

$$\tilde{v} = \eta_x u + \eta_y v \tag{2}$$

where η_x, η_y represent the direction cosines to the cell-face normal.

Assume that this cell face is located on an impermeable boundary so that $\tilde{v} = 0$. We see from Eq. (1) that the only quantity required to compute the flux vector at such a face is the surface pressure. For a cell-centered scheme there are several ways to evaluate this pressure. The most common approach is to extrapolate from the interior of the field. A first-order pressure extrapolation is often used whereby the wall pressure is taken as the value associated with the nearest cell center. A second-order pressure extrapolation is also used with the wall pressure linearly extrapolated from the two nearest cell centers.

Another related approach considered here involves extrapolating the surface pressure such that the normal momentum equation is satisfied. At the surface, the normal momentum equation may be written as:

$$\left(\frac{\partial p}{\partial n}\right)_w = -\rho q^2/R \tag{3}$$

where n is the direction normal to the wall, q is the magnitude of the velocity, and R is the radius of curvature of the wall. In applying this condition for grids which are orthogonal to the body surface, we use a quadratic extrapolation of the pressure involving the values of p from the two nearest cell centers along with the value of $\partial p/\partial n$ taken from Eq. (3) with ρ and q evaluated at the first cell center from the wall. We will denote this procedure as the normal-momentum pressure extrapolation.

As stated with Eq. (1) the evaluation of the surface flux only requires a specification of the wall pressure. However, it is often desirable to know the remaining surface quantities at the wall. For the pressure extrapolation procedures, a model is often used whereby the surface values of entropy and stagnation enthalpy are assumed to be equal to those at the first cell center from the wall. These conditions along with the impermeability condition $\tilde{v} = 0$ can be used to find surface values of all flow variables.

The extrapolation techniques can result with a possible inconsistency for supersonic flows with embedded oblique shocks, since such a shock may lie between the surface and the nearest cell centers, even in the limit of vanishing cell size. In Ref. 13, the present authors utilized a characteristic boundary condition, which was written as:

$$p_w = p_1 \pm \rho_1 a_1 \tilde{v}_1 \tag{4}$$

where subscripts w and 1 refer to the wall and the nearest cell center, respectively, with a being the speed of sound and the plus and minus signs applying to upper and lower walls, respectively. (An upper wall may be considered to be a wall which is located in the downstream $\tilde{v}$ direction from the flow.) Equation (4) evolves from an approximation to the one-dimensional characteristic compatibility relationship in the (η, t) plane. The streamwise compatibility relations yield $\rho_w = -\rho_1 - (p_1 - p_w)/a_1^2$ and $\tilde{u}_w = \tilde{u}_1$, which along with $\tilde{v}_w = 0$ will define all the flow variables at the wall.

Shock Reflection Problem

A problem which illustrates the importance of the characteristic boundary condition is the reflection of an oblique shock at a flat plate. We consider a freestream Mach number of 2.9 with an incident shock angle equal to -29 deg. The computation has been performed using an algorithm based on the flux-difference splitting of Roe[16] with nominal second-order spatial accuracy. A uniform 61×33 grid in a rectangular region of length 2.75 and height of 1.0 has been used.

Results with Classical Surface Conditions

In Fig. 1 we present the pressure distribution along the wall in the shock reflection region including the exact solution, results computed with first-order (P-I), second-order (P-II) and normal momentum pressure extrapolations, along with results computed with the characteristic boundary condition. We see that the characteristic boundary condition gives a smooth distribution, whereas the pressure extrapolations result in oscillations and overshoots downstream of the shock. Similar conclusions can be drawn from the isobar patterns for these case with Figs. 2a–2c corresponding to the three pressure extrapolations and Fig. 2d corresponding to the characteristic boundary conditions. The overshoot in surface pressure is evident downstream of the reflected shock for the pressure-extrapolation cases. The characteristic boundary condition produces a smooth result along the surface but indicates the presence of an overshoot or wiggles in the direction normal to the wall, just upstream of the shock intersection. Also the isobars near the surface for both the characteristic boundary-condition case and the second-order pressure-extrapolation case do not have the correct slope, which should be $\partial p/\partial n = 0$ for a flat wall.

We can get some insight into the behavior of the surface boundary condition by noting that for an inviscid flow, the oblique shock reflection from a flat plate is equivalent to the

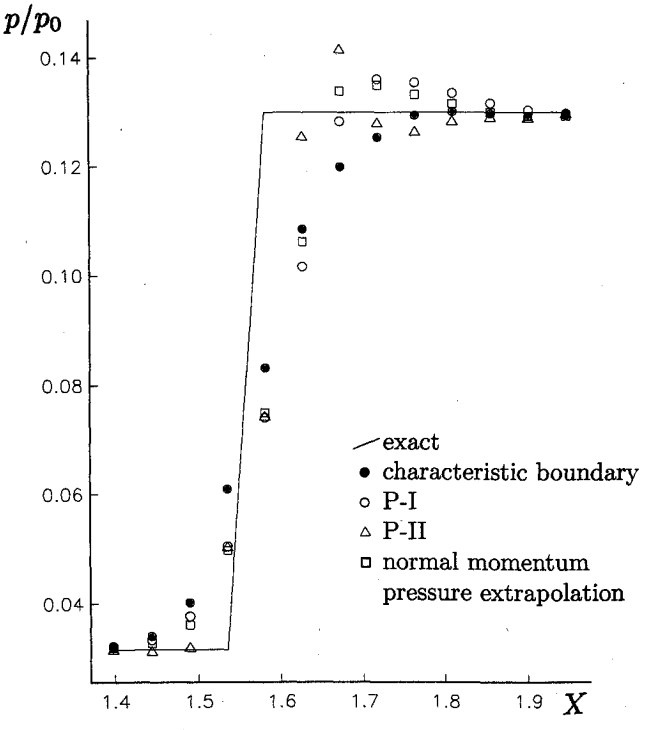

Fig. 1 Surface pressure distribution—shock reflection problem.

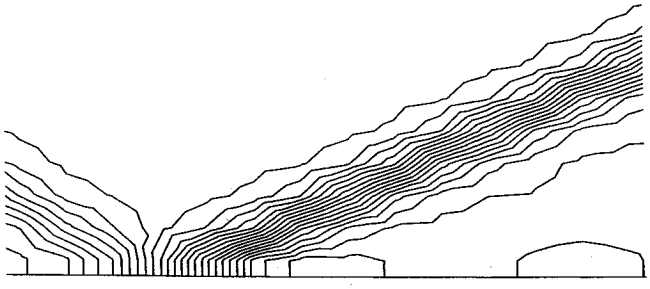

Fig. 2a Pressure contours—shock reflection problem: first-order pressure extrapolation *P*-I.

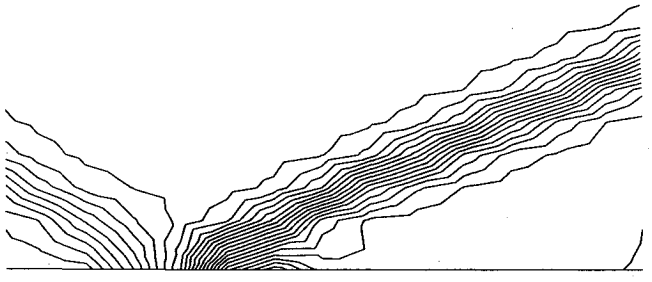

Fig. 2b Pressure contours—shock reflection problem: second-order pressure extrapolation *P*-II.

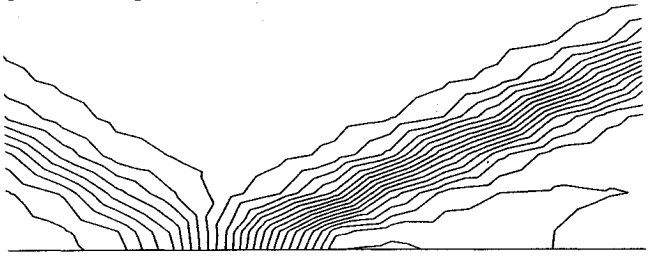

Fig. 2c Pressure contours—shock reflection problem: normal momentum pressure extrapolation.

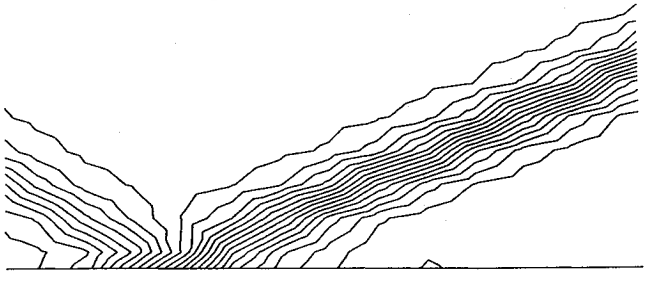

Fig. 2d Pressure contours—shock reflection problem: characteristic boundary condition.

problem of the interaction of two symmetric oblique shocks. The flow conditions along the line of symmetry between the shocks should be identical to the flow conditions along the flat plate. This full-plane problem does not require any special procedures to be applied at the symmetry line. The computed isobars for the equivalent problem are shown in Fig. 3. We see that there are no wiggles or overshoots in directions along the symmetry line or normal to the symmetry line and $\partial p/\partial n$ is zero. Consideration of these results forms the motivation for the approach which we discuss next.

Characteristic Boundary Condition from Roe's Method

We first consider a cell face located on the surface of a plane wall or along the interface of the equivalent symmetric problem. When solving the full-plane problem by an approximate Riemann solver, the left and right states at such an interface are characterized by the same values of pressure, density, and velocity component parallel to the wall and by antisymmetric values of the velocity component normal to the wall. When solving the half-plane problem, this symmetry may be taken into account in the following manner. After having determined the right (or left) states from the interior of the computational flowfield, the left (or right) states may be evaluated by enforcing:

$$\begin{aligned} p_\ell &= p_r \\ \rho_\ell &= \rho_r \\ \tilde{u}_\ell &= \tilde{u}_r \\ \tilde{v}_\ell &= -\tilde{v}_r \end{aligned} \tag{5}$$

where $\tilde{v}$ is the velocity component normal to the wall and $\tilde{u}$ is the velocity component parallel to the wall. The left state (subscript ℓ) refers to the side of the cell edge in the direction towards lower index number and the right state (subscript r) towards higher index number.

The approximate solution of the Riemann problem, using Roe's method (e.g., Ref. 16), along with Eqs. (5) gives the following relations:

$$\tilde{v}_w = 0 \tag{6}$$

and

$$p_w = p_r + \rho_r \tilde{v}_r [\tilde{v}_r - a_w] \tag{7}$$

where $a_w^2 = (\gamma - 1)(H_r \dot{-} \tilde{u}_r^2/2)$, with H being the total enthalpy. Equation (6) enforces the impermeability condition and Eq. (7) is the evaluation of the pressure used to compute the surface flux. Comparison of Eq. (7) with Eq. (4) indicates that this relationship can be considered as characteristic boundary condition for plane walls within the framework of Roe's method.

The shock reflection test case has been recomputed by using the given characteristic boundary condition, Eq. (7). The isobar patterns, not presented here, are quite similar to those plotted in Fig. 2d and, in particular, show again some small oscillations in the direction normal to the plate, so that no major improvement seems to have been obtained with this boundary condition.

Wall Pressure

At this stage a natural question comes into mind: which is the pressure at the wall? A simple and immediate answer could bring us to state the pressure used to compute the surface flux to be the pressure at the wall. These values of pressure have been employed to determine the isobar patterns in Figs. 2a–2d.

However, we can get some insight on the problem by considering the isobar pattern for the full-plane problem, Fig. 3, (which did not require any special treatment on the symmetry

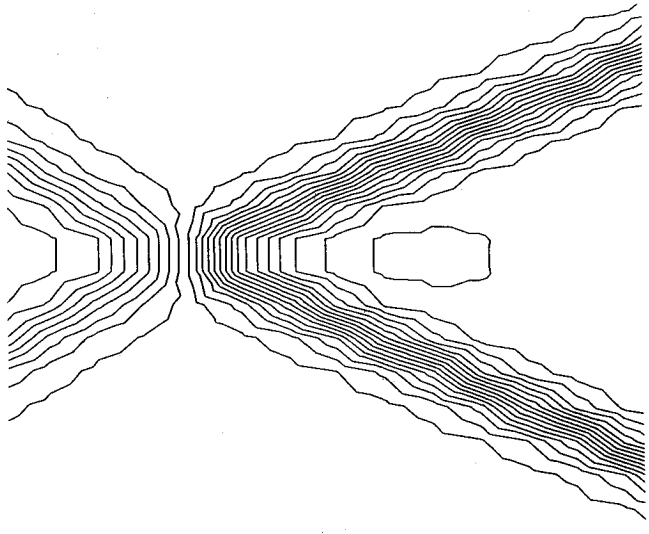

Fig. 3 Pressure contours—full-plane (equivalent) interaction problem.

line). We have compared the results for the full-plane calculation with the results from the wall calculation using the characteristic boundary condition given by Eq. (7). It appears that over most of the flowfield the results are very similar. The major discrepancy occurs right at the surface. The value of the pressure used in the flux calculation, given by Eq. (7), is far from the value which may be inferred from the isobar pattern in the full-plane problem.

One possible reason for this discrepancy may be associated with the fact that the isobar patterns are calculated with cell-area-averaged values everywhere except at the surface itself, where cell-edge-averaged values are used. Another possible reason may be associated with the methods used in the application of the approximate Riemann solution for the evaluation of the surface flux. This flux is computed from discontinuous left and right states of the flow variables at a cell edge. The value of the surface flux from the approximate Riemann solver, although appropriate for the time integration of the solution for the cell-averaged conserved variables, may not accurately represent the surface pressure.

This reasoning leads us to propose boundary-condition procedures having two parts. The first part consists of the evaluation of the surface flux in as consistent a manner as possible with those on cell edges interior to the domain, such as that given by Eqs. (5-7). The second part consists of an evaluation of the surface pressure extrapolated from interior cell-area-averaged values and consistent with the normal momentum equation evaluated at the surface, Eq. (3). The purpose of the evaluation of pressure using the second part of our procedure is for data presentation purposes, e.g., isobars, wall pressures, lift and drag, etc. The computation itself uses the surface fluxes from the first part of the procedure.

New Boundary Condition Procedures

In this section we consider two new procedures for implementing surface boundary conditions in a finite-volume Euler computation. The methods are motivated by consideration of the full-plane problem and the preceding remarks on the wall pressure. The first method, strictly valid for steady flows over planar walls, is called the symmetry technique (ST).

Symmetry Technique

For the grid sketched in Fig. 4, we locate two image cells below the surface, outside the computational domain. The cell-averaged values of the pressure, density, and the velocity component parallel to the wall are taken symmetrically from their values in the interior of the computational domain, whereas antisymmetric conditions are enforced for the normal velocity component. Namely, with the cell indexed as indicated on Fig. 4,

$$\begin{aligned} p_{-1} &= +p_1, \quad p_{-2} = +p_2 \\ \rho_{-1} &= +\rho_1, \quad \rho_{-2} = +\rho_2 \\ \tilde{u}_{-1} &= +\tilde{u}_1, \quad \tilde{u}_{-2} = +\tilde{u}_2 \\ \tilde{v}_{-1} &= -\tilde{v}_1, \quad \tilde{v}_{-2} = -\tilde{v}_2 \end{aligned} \tag{8}$$

Thus no special treatment is required for the flux evaluation at the surface, since, with the specification of the image cells,

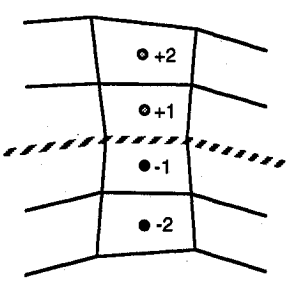

Fig. 4 Image cells for symmetry technique.

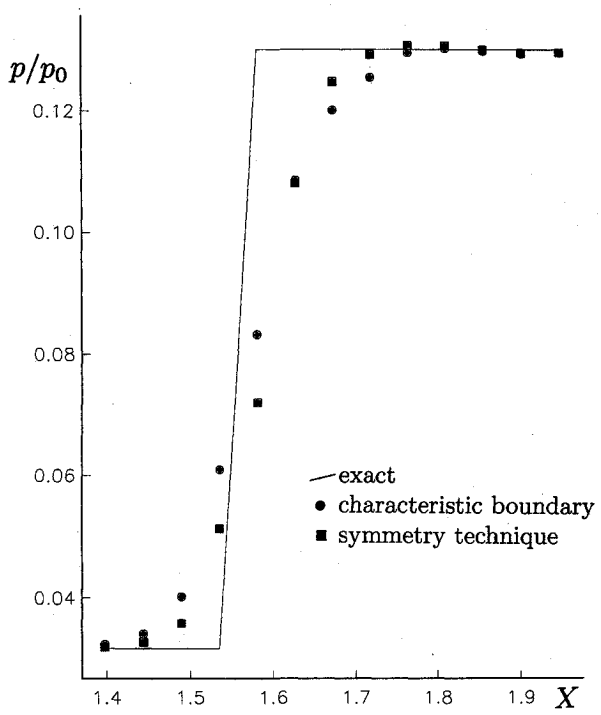

Fig. 5 Surface pressure distribution—shock reflection problem: characteristic boundary condition and symmetry technique ST.

the surface flux may be computed as any other cell face. However, with the specification of the image value given in Eq. (8), the impermeability condition, Eq. (6) is automatically satisfied and the pressure used to compute the fluxes across this interface will be, in effect, given by Eq. (7).

There are several advantages associated with using this type of reflection boundary condition as opposed to the characteristic boundary condition implementation associated with actually using Eq. (7). Firstly, limiters can be implemented, just as with any internal cell-face flux evaluation. The use of the limiters is important near the shock intersection with the wall. Also, this procedure allows for second-order spatial accuracy for both the surface cell face and the first cell face off the surface. (In applying any other boundary condition procedure, the left state for the first cell face off the surface cannot be computed with complete second-order accuracy.) It may also be noted that the physical location of the image-cell geometry does not affect the computation.

The second part of this boundary condition technique involves computing the physical wall pressure by the normal-momentum extrapolation, as previously described. It should be noted that this value of surface pressure is not used in the computation itself, but is only used for the purposes of presenting the results.

Results for the shock reflection problem using the symmetry technique boundary conditions are presented in Fig. 5. The surface pressure distribution with this boundary condition is smooth and monotonic and compares favorably with the characteristic boundary condition. The pressure contours, not shown here, precisely duplicate one half of the full-plane contours of Fig. 3 and give an excellent representation of the flowfield, without any of the oscillations or overshoots associated with the other boundary conditions in Figs. 2a–2d.

Curvature-Corrected Symmetry Technique

The symmetry technique for solid wall boundary conditions does not take into account the wall curvature. A method which addresses this issue, which we call the curvature-corrected symmetry technique (CCST), is based on utilizing the normal-momentum equation, Eq. (3), to account for surface curvature.

In this procedure, we again incorporate the system of image cells, illustrated in Fig. 4, but we do not utilize the symmetry conditions given in Eqs. (8). Instead, the pressure at the image points is determined from an integration of Eq. (3) which we approximate as

$$p_{-1} = p_1 - \rho_w \frac{q_w^2}{R} \Delta n_1$$
$$p_{-2} = p_2 - \rho_w \frac{q_w^2}{R} \Delta n_2 \tag{9}$$

where Δn_1 represents the distance between cell center 1 and the image-cell center -1, and likewise Δn_2 is the distance between 2 and -2.

The other flow quantities may be evaluated by locally modeling the inviscid flow over a solid surface as a vortex flow of constant entropy and total enthalpy. Thus in addition to the pressure condition given by Eq. (9), we also assume symmetric values of the entropy and total enthalpy. For a perfect gas, it is easily shown that the preceding conditions lead to

$$\rho_{-1} = \rho_1 \left(\frac{p_{-1}}{p_1}\right)^{1/\gamma}$$
$$\rho_{-2} = \rho_2 \left(\frac{p_{-2}}{p_2}\right)^{1/\gamma} \tag{10}$$

and

$$\tilde{u}_{-1}^2 = \tilde{u}_1^2 + \frac{2\gamma}{\gamma - 1}\left(\frac{p_1}{\rho_1} - \frac{p_{-1}}{\rho_{-1}}\right) + \tilde{v}_1^2 - \tilde{v}_{-1}^2$$
$$\tilde{u}_{-2}^2 = \tilde{u}_2^2 + \frac{2\gamma}{\gamma - 1}\left(\frac{p_2}{\rho_2} - \frac{p_{-2}}{\rho_{-2}}\right) + \tilde{v}_2^2 - \tilde{v}_{-2}^2 \tag{11}$$

where γ is the constant ratio of specific heats. The remaining condition stems from the impermeability condition. This condition is enforced by selecting $\tilde{v}_{-1}$ and $\tilde{v}_{-2}$ such that the Roe-averaged value of the normal velocity $\tilde{v}$ is zero at the surface. This is accomplished by setting $\tilde{v}_{-1} = -\tilde{v}_1$ and choosing $\tilde{v}_{-2}$ such that $\tilde{v}_\ell \sqrt{\rho_\ell} + \tilde{v}_r \sqrt{\rho_r} = 0$. In the absence of limiters, using linear extrapolations for the left and right states results in

$$\tilde{v}_{-1} = -\tilde{v}_1$$
$$\tilde{v}_{-2} = 3\tilde{v}_{-1} + 2[\tilde{v}_1 + (\tilde{v}_1 - \tilde{v}_2)/2] \sqrt{\frac{\rho_1 + (\rho_1 - \rho_2)/2}{\rho_{-1} + (\rho_{-1} - \rho_{-2})/2}} \tag{12}$$

We may note that for a flat surface, the radius of curvature $R \to \infty$ so that Eqs. (9–12) reduce to the symmetry conditions given in Eqs. (8). Thus the two procedures are actually based on the same model for the determination of the image-cell quantities.

In the curvature-corrected symmetry technique we also calculate a value of surface pressure by what we have called a normal-momentum pressure extrapolation. This condition involves a quadratic extrapolation of the pressure using the values of p from the two nearest cell centers (p_1 and p_2 in Fig. 4), along with the value of $\partial p/\partial n$ taken from Eq. (3). We obtain

$$p_w = \left[p_1 \Delta n_2^2 - p_2 \Delta n_1^2 - \rho_w \frac{q_w^2}{2R} \Delta n_1 \Delta n_2 (\Delta n_2 - \Delta n_1) \right] \Big/ (\Delta n_2^2 - \Delta n_1^2) \tag{13}$$

It should be again noted that this value of surface pressure is not used in the computation itself, but is only used for the purposes of presenting the results. The remaining surface flow quantities may be determined by modeling the surface values of entropy and stagnation enthalpy equal to those at the first cell center from the wall. The preceding implementation of the normal-momentum pressure extrapolation is valid for grids which are orthogonal to the surface. Normal-momentum pressure extrapolations for nonorthogonal grids have been addressed by Rizzi[9] and have not been considered within the present context.

It should be noted that for the evaluation of the image points in Eqs. (9) and for the wall pressure extrapolation, Eq. (13), we generally take $\rho_w = \rho_1$ and $q_w = \tilde{u}_1$. This avoids extrapolations across discontinuities and, in our experience, has a minimal effect on the results. In addition, we generally implement Eq. (9) neglecting the effect of grid variation by taking $\Delta n_2 = 3\Delta n_1$. This also has been noted to have a minimal effect on the results and is consistent with neglecting this effect in the monotone upwind scheme for scalar conservation laws (MUSCL) extrapolations. In the same spirit, we also neglect the mesh variation in applying all the pressure-extrapolation procedures discussed in the preceding sections.

Results

We have considered several test cases to evaluate the new boundary condition approaches. The most compelling example, the subsonic compressible flow over a circular cylinder, will be presented here. Other cases, including the supersonic blunt-body problem, appear in Ref. 17.

We considered a freestream Mach number of $M_\infty = 0.38$ inviscid flow over a circular cylinder. This flow condition produces a maximum Mach number of approximately 0.92 on the surface of the cylinder. We computed the flowfield using three polar grids: 32×8, 64×16, and 128×32. For each grid, the larger number corresponds to the number of cells uniformly spaced in the circumferential direction, over an extent of 360 deg. The smaller number corresponds to the number of cells in the radial direction uniformly stretched to a far field located at 20 diameters. The minimum radial cell dimension ranged from 0.1252 diameter for the coarsest grid, to 0.0531 diameter for the middle grid, to 0.0245 diameter for the finest grid. Again computations were performed using the pressure extrapolations P-I and P-II and the symmetry techniques, ST and CCST.

We considered a variety of parameters to compare the effectiveness of these methods. The first parameter is the value of surface pressure at the top of the cylinder ($\theta = 90$ deg), denoted the minimum pressure in Fig. 6a for the four boundary

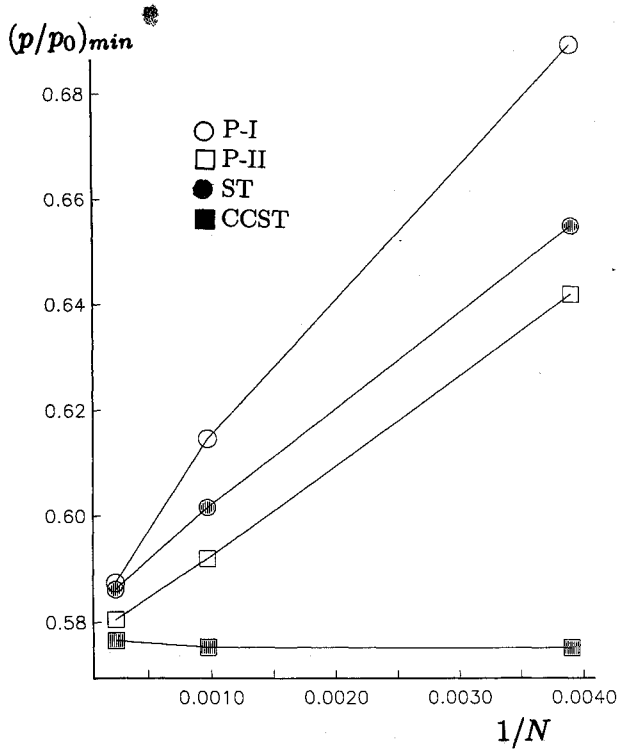

Fig. 6a Minimum surface pressure—subsonic cylinder problem.

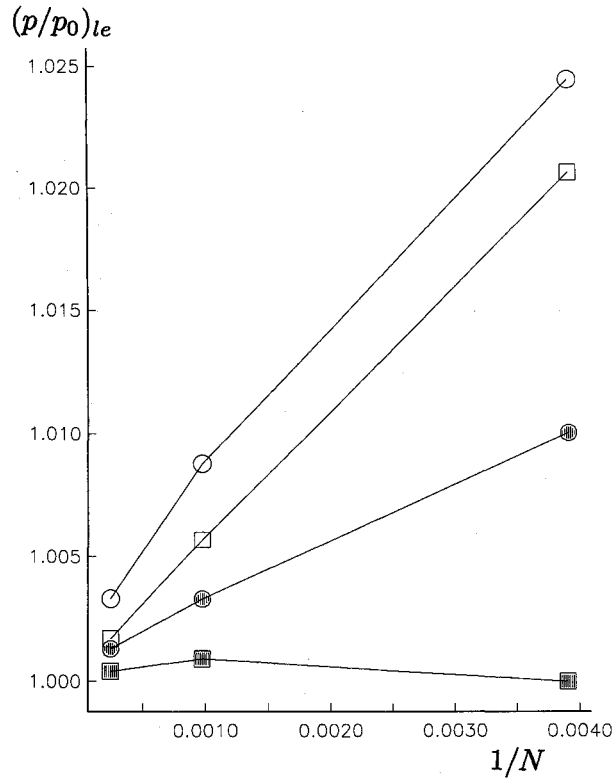

Fig. 6b Leading-edge pressure—subsonic cylinder problem.

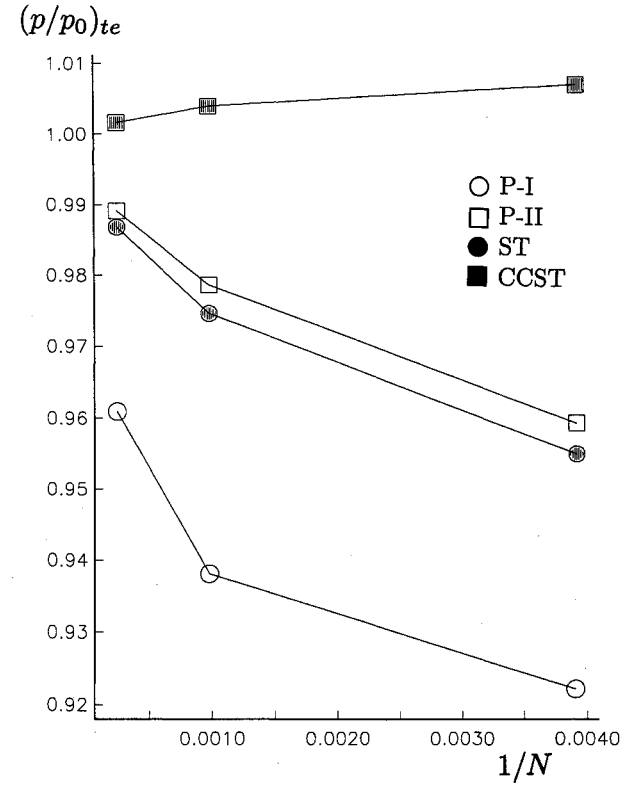

Fig. 6c Trailing-edge pressure—subsonic cylinder problem.

procedures plotted against the inverse of the total number of cells. From these results it appears that all the methods are consistent and approach nearly the same pressure value in the limit of vanishing cell size. However, the CCST results are remarkably converged in grid, with apparently accurate results even at the coarsest grid level. The CCST results appear to be significantly more accurate than the other approaches with the ST having similar accuracy as the second-order P-II and the first-order P-I being the least accurate.

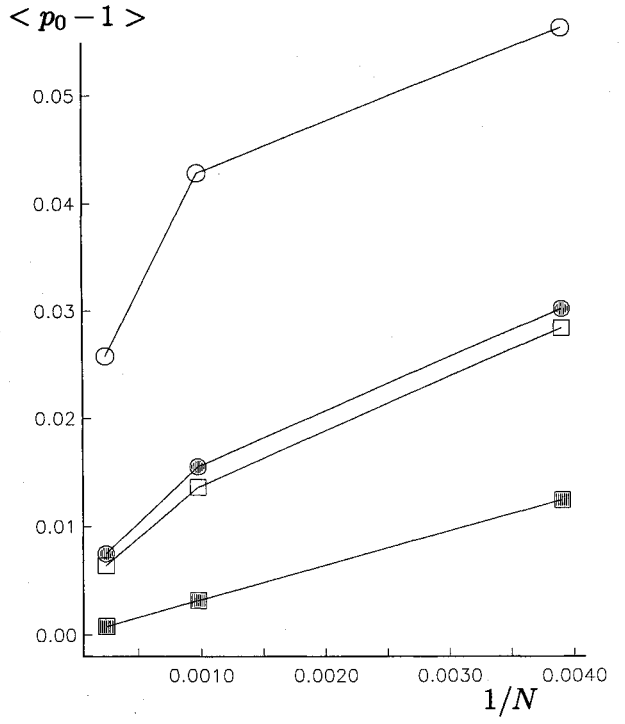

Fig. 6d $\mathcal{L}_2$-norm of surface total pressure—subsonic cylinder problem.

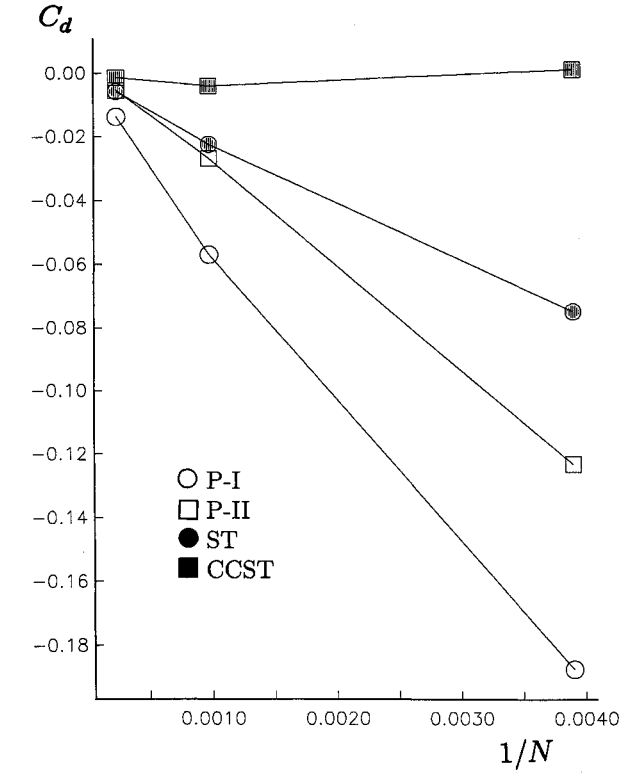

Fig. 6e Drag coefficient—subsonic cylinder problem.

Other results confirming the remarkable behavior of the CCST are presented in Figs. 6b–6e. The leading-edge pressure vs grid size shown in Fig. 6b confirms the remarkable grid convergence of CCST and illustrates the consistency between the methods as the mesh size vanishes. The trailing-edge pressure results in Fig. 6c also confirm the grid convergence of the CCST but also indicate improved accuracy of this method even at fine grids. We see that P-II and ST have about a 1% error in trailing-edge pressure and P-I has nearly a 4% error, in contrast to the error in pressure at the trailing edge for the CCST, which is approximately 0.1%. In Fig. 6d we present a

measure of the $\mathcal{L}_2$ norm of the total pressure error on the surface of the body. The improvement in accuracy of the CCST is evident for all grid levels. Similar conclusions may be drawn from the drag coefficient presented in Fig. 6e where remarkably low values of c_d, ranging from 0.0014 on the coarsest grid to -0.0014 on the finest grid, were obtained with the CCST.

Next we present the Mach number contours and entropy contours for fine-mesh results using the four approaches in Figs. 7–10. The Mach number contours are spaced at $\Delta M = 0.1$ and the entropy contours are spaced at $\Delta s = 0.001$. The first-order pressure extrapolation technique P-I produces the most distorted Mach number pattern downstream of the cylinder, shown in Fig. 7a. This method also generated the highest spurious entropy levels on the aft portion of the cylinder as indicated in Fig. 7b with $s_{\max} > 0.017$. The results from P-II shown in Figs. 8a and 8b and the results from the ST shown in Figs. 9a and 9b have slightly improved downstream Mach number contours and generate less entropy with values of $s_{\max} > 0.007$ for P-II and values of $s_{\max} > 0.005$ for the ST. However, the results for CCST in Figs. 10a and 10b are in stark contrast, with a nearly symmetric Mach number pattern and extremely minute values of spurious entropy with $s_{\max} < 0.001$.

The supersonic blunt-body results reported in Ref. 17 indicated that the symmetry techniques, both with and without curvature correction, were in better agreement with benchmark results than those using the pressure-extrapolation procedures and that the ST performed nearly as well as the CCST. For the subsonic cylinder problem, the CCST was clearly superior to the ST. We may explain this discrepancy by noting that on the front portion of the subsonic cylinder, where the flow is constantly expanding, the flowfield results for the ST are nearly as good as that for the CCST. Another point that

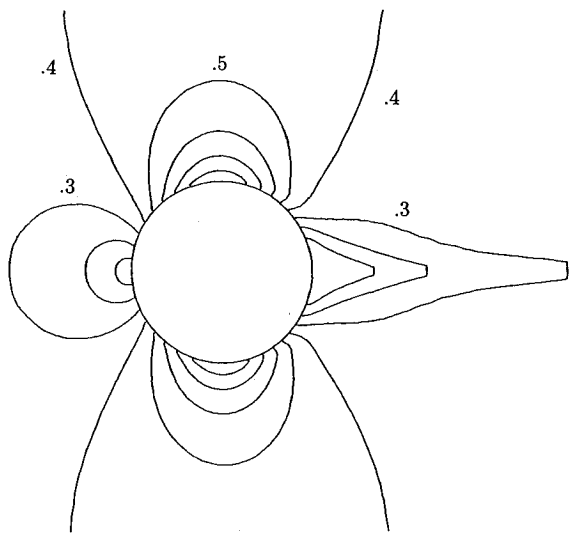

Fig. 7a Mach number contours—subsonic cylinder problem: first-order pressure extrapolation P-I.

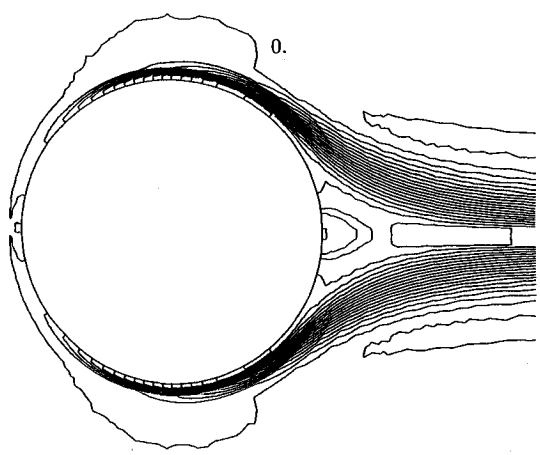

Fig. 7b Entropy contours—subsonic cylinder problem: first-order pressure extrapolation P-I.

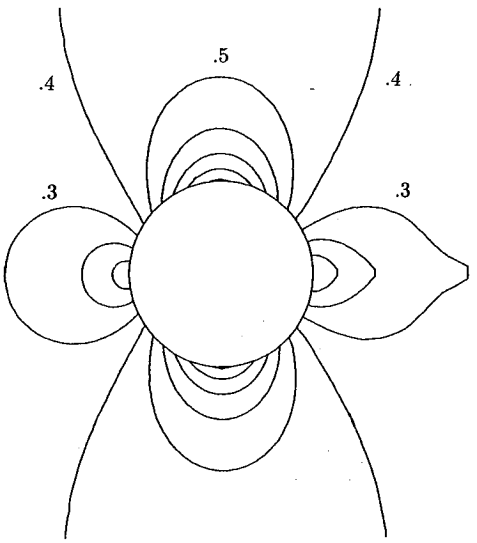

Fig. 8a Mach number contours—subsonic cylinder problem: second-order pressure extrapolation P-II.

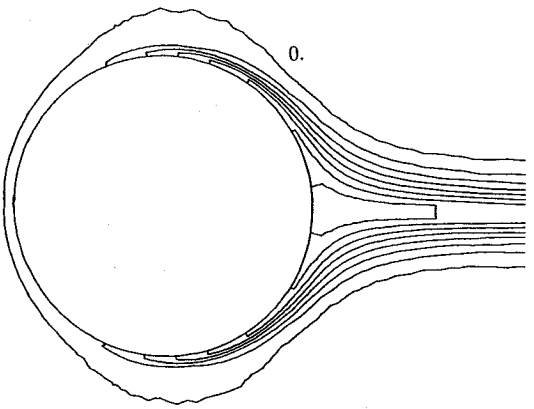

Fig. 8b Entropy contours—subsonic cylinder problem: second-order pressure extrapolation P-II.

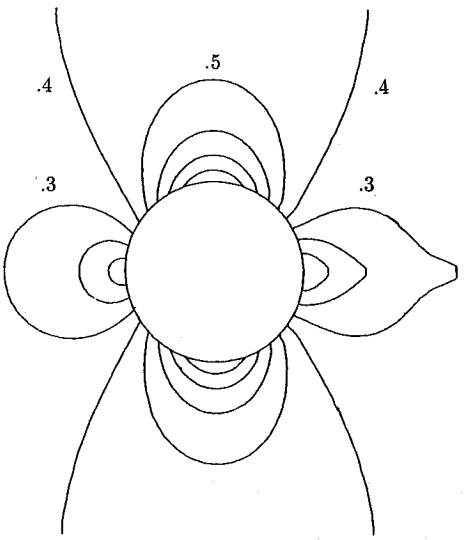

Fig. 9a Mach number contours—subsonic cylinder problem: symmetry technique ST.

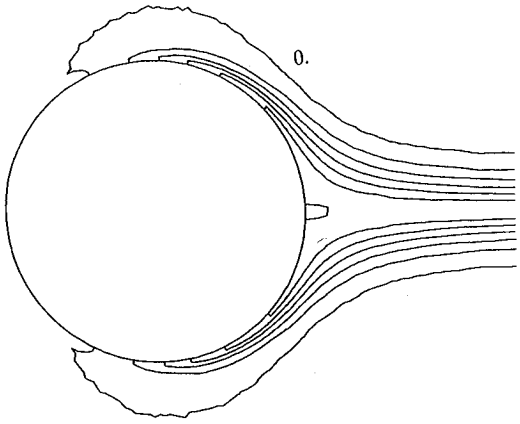

Fig. 9b Entropy contours—subsonic cylinder problem: symmetry technique ST.

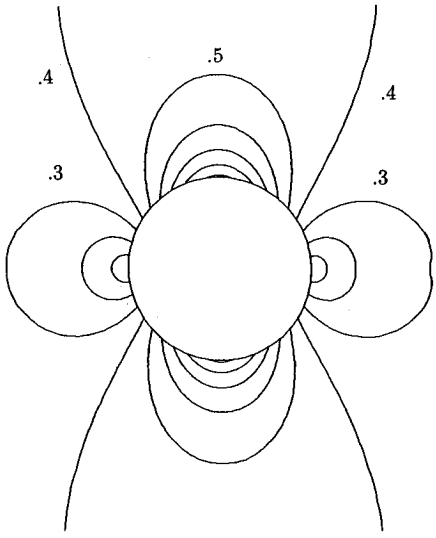

Fig. 10a Mach number contours—subsonic cylinder problem: curvature-corrected symmetry technique CCST.

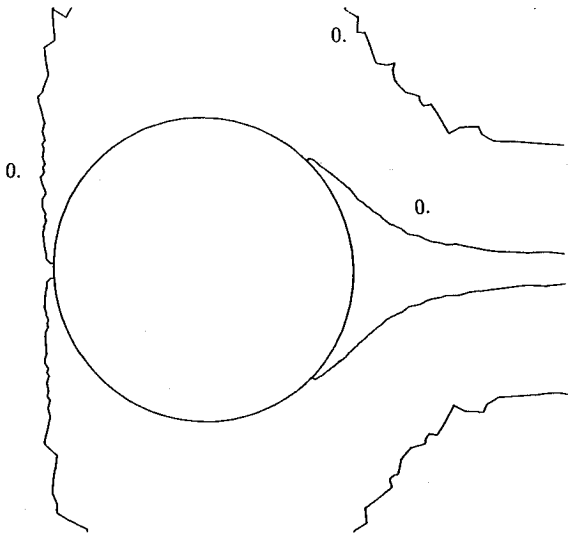

Fig. 10b Entropy contours—subsonic cylinder problem: curvature-corrected symmetry technique CCST.

we might mention is that this procedure has been adapted by Catalano et al.[18] for use in a cell-vertex scheme in conjunction with a multidimensional Riemann solver. Excellent symmetric results were presented for the subsonic flow over a circular bump, which could not be achieved with other boundary condition procedures. Results were obtained using the CCST at very low Mach numbers using a preconditioned Euler code by Godfrey et al.[19] Applications of the symmetry technique have also been made in conjunction with the nonconservative λ scheme in Ref. 14 and with a multidirectional Riemann solver in Ref. 20.

Conclusions

We have considered the implementation of boundary conditions at solid walls in steady, inviscid Euler solutions by flux-difference-split, finite-volume methods. First we indicated the breakdown of standard pressure-extrapolation procedures for the problem of an oblique shock reflecting off a planar surface. We showed the importance of using characteristic boundary conditions and a method of applying the classical flux-difference splitting of Roe as a characteristic boundary condition. Consideration of the equivalent problem of the intersection of two (equal and opposite) oblique shocks was very illuminating on the role of surface boundary conditions for an inviscid flow. The equivalent problem also served to clarify the differences between the pressure which a finite-volume flow solver uses to evaluate the surface flux and the surface pressure. These considerations led to the introduction of two new boundary-condition procedures, denoted the symmetry technique and the curvature-corrected symmetry technique. Examples of the effects of the various surface boundary conditions were considered for the subcritical compressible flow over a circular cylinder. Dramatic advantages of the curvature-corrected symmetry technique over the other methods are shown, particularly with regard to numerical entropy generation, total pressure loss, drag, and grid convergence. In addition, recent evidence indicates that the two symmetry techniques are applicable to a variety of other Euler formulations.

Acknowledgments

The research of A. Dadone was supported by the Italian agency Ministers della Ricera Scientifica e Tecnologica. B. Grossman acknowledges the assistance of the National Science Foundation under the U.S.-Italy Cooperative Science Program, Grant INT-8814895 and the National Aeronautics and Space Administration under NASA Langley Grant NAG-1-776.

References

[1]Moretti, G., "Importance of Boundary Conditions in the Numerical Treatment of Hyperbolic Equations," *High-Speed Computing in Fluid Dynamics, Physics of Fluids,* Supplement II, 1969, pp. II-13–II-20.

[2]Burstein, S. Z., "Numerical Methods in Multidimensional Shocked Flows," *AIAA Journal,* Vol. 2, No. 12, 1964, pp. 2111–2117.

[3]Moretti, G., and Abbett, M.,"A Time-Dependent Computational Method for Blunt Body Flows," *AIAA Journal,* Vol. 4, No. 12, 1966, pp. 2136–2141.

[4]Kentzer, C. P., "Discretization of Boundary Conditions on Moving Discontinuities," *Lecture Notes in Physics,* No. 8, Springer-Verlag, New York, 1970, pp. 108–113.

[5]De Neef, T., "Treatment of Boundaries in Unsteady Inviscid Flow Computations," Delft Univ. of Technology, Dept. of Aerospace Engineering, Rept. LR-262, Delft, The Netherlands, Feb. 1978.

[6]Moretti, G., "The λ-Scheme," *Computers and Fluids,* Vol. 7, 1979, pp. 191–205.

[7]Chakravarthy, S. R., "Euler Equations—Implicit Schemes and Boundary Conditions," *AIAA Journal,* Vol. 21, No. 5, 1983, pp. 699–706.

[8]Marcum, D. L., and Hoffman, J. D., "Numerical Boundary Condition Procedures for Euler Solvers," *AIAA Journal,* Vol. 25, No. 8, 1987, pp. 1054–1068.

[9]Rizzi, A., "Numerical Implementation of Solid Boundary Conditions for the Euler Equations," *Z.A.M.M.,* Vol. 58, No. 7, 1978, pp. T301–T304.

[10]Walters, R. W., and Thomas, J. L., "Advances in Upwind Relaxation Methods," *State-of-the-Art Surveys of Computational Mechanics,* edited by A. K. Noor, American Society of Mechanical Engineers Publication, New York, 1988, Chap. 4.

[11]Clark, D. K., Salas, M. D., and Hassan, H. A., "Euler Calculations for Multielement Airfoils Using Cartesian Grids," *AIAA Journal,* Vol. 24, No. 3, 1986, pp. 353–358.

[12]Deconinck, H., and Struys, R., "Consistent Boundary Conditions for Cell-Centered Upwind Finite-Volume Euler Solvers," *Numerical Methods for Fluid Dynamics III,* edited by K.W. Morton and M. J. Baines, Clarendon Press, Oxford, England, UK, 1988, pp. 464–470.

[13]Dadone, A., and Grossman, B., "A Rotated Upwind Scheme for the Euler Equations," AIAA Paper 91-0635, Jan. 1991; also "Characteristic-Based, Rotated Upwind Scheme for the Euler Equations," *AIAA Journal,* Vol. 30, No. 10, 1992, pp. 2219–2226.

[14]Dadone A., "A Physical-Numerical Treatment of Impermeable Boundaries in Compressible Flow Problems," *Proceedings of the Fourth International Symposium on Computational Fluid Dynamics* (Davis, CA), Sept. 1991, Vol. I, Univ. of California, Davis, CA, pp. 258–263.

[15]Dadone, A., "A Numerical Technique to Compute Euler Flows at Impermeable Boundaries Based on Physical Considerations," *Proceedings of the IV International Conference on Hyperbolic Problems,* (Taormina, Italy), April 1992; also *Notes on Numerical Fluid Dynamics,* Vol. 43, Vieweg, Braunsweig, Germany, 1993, pp. 171–178.

[16]Roe, P. L., "Characteristic-Based Schemes for the Euler Equations," *Annual Review of Fluid Mechanics,* Vol. 18, 1986, pp. 337–365.

[17]Dadone, A. and Grossman, B., "Surface Boundary Conditions for the Numerical Solution of the Euler Equations," *Proceedings of the AIAA 11th Computational Fluid Dynamics Conference* (Orlando, FL), AIAA, Washington, DC, 1993, pp. 411–422 (AIAA Paper 93-3303-CP).

[18]Catalano, L. A., De Palma, P., and Pascazio, G., "A Multi-Dimensional Solution Adaptive Multigrid Solver for the Euler Equations," *Proceedings of the Thirteenth International Conference on Numerical Methods in Fluid Mechanics* (Rome, Italy), July 1992, *Lecture Notes in Physics,* Vol. 414, Springer-Verlag, Berlin, Germany, pp. 90–94.

[19]Godfrey, A. G., Walters, R. W., and Van Leer, B., "Preconditioning for the Navier-Stokes Equations with Finite-Rate Chemistry," AIAA Paper 93-0535, Jan. 1993.

[20]Dadone, A., and Grossman, B., "A Multidimensional Upwind Scheme for the Euler Equations," *Proceedings of the Thirteenth International Conference on Numerical Methods in Fluid Mechanics* (Rome, Italy), July 1992, *Lecture Notes in Physics,* Vol. 414, Springer-Verlag, Berlin, Germany, pp. 95–99.